Yaxu Zheng, Fuming Wang*, Changrong Li, Yu Lin and Ruifang Cao

Effect of Martensite Structure and Carbide Precipitates on Mechanical Properties of Cr-Mo Alloy Steel with Different Cooling Rate

https://doi.org/10.1515/htmp-2018-0018
Received February 02, 2018; accepted June 08, 2018

Abstract: The effect of cooling rate on martensitic structure and carbides precipitation behavior was investigated based on Cr-Mo alloy steel with different quenching media of oil, water and 10% NaCl-water, respectively. The influence mechanism of martensite structure and carbide precipitates on mechanical properties was also studied. The results showed that martensite packets and blocks were refined with water quenching, however, they were coarse with oil or 10% NaCl-water quenching. Martensite laths were refined and dislocation density increased with increasing cooling rate. The carbides in tempered steel were coarse obviously with 10% NaCl-water quenching. The impact toughness deteriorated significantly with 10% NaCl-water quenching due to coarsening of martensite structure and carbides.

Keywords: Cr-Mo alloy steel, martensite structure, carbide precipitates, mechanical property, cooling rate

Introduction

The steel 25CrMo is used for axle on high-speed trains in China. The axle requires a higher hardenability to reduce the amount of large size ferrite on cross section of axle, since the large size ferrite reduces fatigue strength of axle. The main factors that have influence on hardenability of steel are chemical composition, grain size and cooling rate. Normally, hardenability can be improved with boron addition, large grain size and fast cooling rate [1–7].

Cooling rate not only has influence on hardenability, but also on structure, precipitates and mechanical properties of steel. Shanmugam [8] studied the effect of cooling rate on microstructure and mechanical properties of Nb microalloyed steel and found that the yield strength was improved with increasing cooling rate, while the toughness was not deteriorated. However, there was no obvious difference of precipitates size with different cooling rate. It should be noted that the structure he obtained with different cooling rate was ferrite-pearlite. Wang [9] studied the toughness of martensite structure on surface of ultra-thick steel plate and found that too fast cooling rate on plate surface resulted in coarsening of martensite packets and blocks. Meanwhile, the dislocation density increased. The coarse martensite structure and high dislocation density reduced toughness. Zhang [10] found that the improvement of toughness of 25CrMo48V resulted from refinement of martensite structure with high angle grain boundaries, and the block is the minimum structure controlling toughness. Long [11] found that martensite block was the effective unit controlling strength, while martensite lath was the minimum unit controlling toughness in 20CrNi2Mo steel. There is still dispute about the minimum effective structure of lath martensite dominating toughness. Besides structure, precipitates characteristic, such as number density, size, type, shape and distribution, also has a considerable influence on strength and toughness. Cheng [12] studied the size and distribution of carbides on different locations of thick steel plate. He found that the carbides precipitating in plate surface were coarse due to high dislocation density resulting from fast cooling rate, while the carbides precipitating in 1/2 thickness of plate were small due to low dislocation density caused by relatively slow cooling rate. The ultimate tensile strength decreased with increasing distance from plate surface.

There are many reports about the effect of cooling rate on structure and precipitates in steel as above-mentioned, but most of them are based on high strength steel whose

***Corresponding author: Fuming Wang,** School of Metallurgical and Ecological Engineering, University of Science and Technology Beijing, Beijing 100083, China, E-mail: wangfuming@metall.ustb.edu.cn
Yaxu Zheng, School of Metallurgical and Ecological Engineering, University of Science and Technology Beijing, Beijing 100083, China; Materials Science and Engineering Department, Carnegie Mellon University, Pittsburgh PA 15213, USA
Changrong Li, School of Materials Science and Engineering, University of Science and Technology Beijing, Beijing 100083, China
Yu Lin, Materials Science and Engineering Department, Carnegie Mellon University, Pittsburgh PA 15213, USA
Ruifang Cao, Rolling operation department, Beijing Shougang Co., LTD., Tangshan 064404, PR. China

microstructure is ferrite, pearlite or bainite. There are few reports about the systematic study on the effect of cooling rate on martensite structure and carbide precipitates of heat treated Cr-Mo alloy steel. Therefore, the aim of this work is to investigate the influence mechanism of cooling rate on mechanical properties of martensite steel. The influence of martensite structure and carbides on strength and toughness has also been discussed.

Materials and methods

The experimental material was melted with a 50 kg vacuum induction furnace and then forged into bars with a diameter of 16 mm. The chemical composition is listed in Table 1. In order to homogenize the microstructure of the material, the steel bars were heated at 920°C for 0.5 h and air-cooled. Then, they were heated at 900°C for 0.5 h and quenched in oil, water and 10% NaCl-water, respectively. Finally, they were tempered at 630°C for 0.5 h and air-cooled. The heat treatment procedure is shown in Figure 1. The order of cooling rate from fast to slow is 10% NaCl-water, water and oil. The martensite structure was obtained with the three quenching media due to the small cross section size of tested steel bars. The effects of different quenching cooling rates on martensite structure, carbide precipitates on tempering and mechanical properties have been investigated.

The morphologies of martensite packets, blocks and laths were observed by field emission scanning electron microscopy (FE-SEM, FEI MLA-250), electron back-scattered diffraction (EBSD, JSM-7800 F, Oxford Nordlys F+) and transmission electron microscopy (TEM, Tecnai G2 F20 S-TWIN), respectively. The EBSD scanning step was 0.1 μm and the total scanning area was about 100 μm × 100 μm to measure the average grain size and misorientation angle distribution of martensite. Thermo-Calc with a database of TCFE6 was used to calculate the equilibrium precipitation in tested steel. The carbide precipitates in tempered steels were analyzed by TEM. The dislocation density values in the samples were measured by X-ray diffraction (XRD, PHILIPS APD-10X, Cu anode) after mechanical polishing. The voltage, current and scanning step size are 40 kV, 40 mA and 0.05 degree, respectively.

The thin foil for TEM observation was twin-jet electro-polished with 5% perchloric acid. The carbon extraction replicas used for TEM observation were plated with a thin carbon film on the sample surface which had been etched with 4% nital. Then, the carbon films were stripped off with 4% nital and collected with copper net. The EBSD samples were electro-polished with 5% perchloric acid. The samples for X-ray diffraction were mechanically polished for detection, and the detection area was 20 mm × 10 mm.

The area fraction of carbides was measured based on TEM photos with help of Image J software. The software calculates area fraction automatically. The area of each carbide was measured by Image J software and the diameter of each carbide was calculated with the measured area. Almost 100 laths were measured for each sample. The lath width was estimated by averaging the 100 laths.

Table 1: The chemical composition of the experimental steels (mass %).

Steel	C	Si	Mn	Cr	Mo	V	Ni	N	O	Nb	B
25CrMoNbB	0.27	0.32	0.73	1.08	0.27	0.06	0.28	0.0020	0.0013	0.04	0.0020

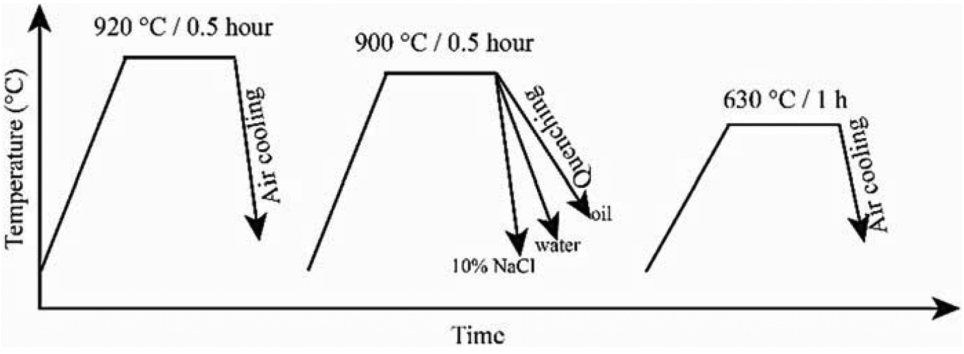

Figure 1: The schematic diagram of heat treatment process.

Maybe the average lath width was not the actual lath width or it was not accurate, since the lath structures were often tilted in the thin film, but the lath width was measured with the same method for all samples. Therefore, the variation trend of the lath width with increasing cooling rate was worth referencing.

The tensile and Charpy impact tests were conducted according to Chinese standard GB/T 228.1–2010 and GB/T 229–2007, respectively. The dimension of tensile and Charpy impact specimens were Φ5 mm × 30 mm and 10 mm × 10 mm × 55 mm, respectively. Five tests were performed for each test condition and the statistical tests of the data were analyzed using box-plot method. The outliers were removed and the average of other data was noted [13].

Results

Martensite structure in the experimental steels

There are several martensite packets within one austenite grain. The packet is composed of blocks, and each block is divided into parallel laths. The schematic diagram of martensite structure is shown in Figure 2. The boundaries of austenite, packets and blocks are high angle, while martensite laths are separated by low angle grain boundaries. Block is the minimum unit with high angle grain boundary in martensite. Therefore, the effective grain size of martensite is the average size of blocks.

The martensite blocks distribution in quenched steels analyzed by EBSD is shown in Figure 3. The black lines represent high angle grain boundaries (HAGB) with larger than 10°. The HAGB boundaries of austenite grains, packets and blocks directly affect the toughness. Block is the minimum unit in martensite structure that controls toughness. The distributions of the grain size and grain boundary misorientation in quenched steels are shown in Figures 4 and 5, respectively. The martensite blocks distribution in tempered steels analyzed by EBSD is shown in Figure 6. As shown in Figure 7 (a), the analysis results show that the effective grain size (average size of blocks) are 1.286 μm, 0.746 μm and 1.002 μm and the fractions of high angle grain boundaries are 35.02%, 37.20% and 36.82% for oil-quenched, water-quenched and 10% NaCl-water-quenched steels, respectively. As shown in Figure 7 (b), the effective grain size are 1.52 μm, 1.21 μm and 1.65 μm and the fractions of high angle grain boundaries are 40.3%, 38.5% and 39.2% for oil-quenched, water-quenched and 10% NaCl-water-quenched and tempered steels, respectively. After tempering, both the effective grain size and the HAGB fraction increase slightly, which is since there are laths combination due to dissolution and dislocation density decrease during tempering. Many low angle boundaries disappear, so the HAGB fraction increases. Some relatively low angle boundaries of blocks also disappear during tempering [13], so the effective size increases lightly. The effective grain size of water-quenched steel is the smallest. However, there is no obvious difference of the fractions of high angle grain boundaries. In addition, the block size of water-quenched steel is more uniform than that of oil-quenched steel or 10% NaCl-water-quenched steel, as shown in Figure 4 (b).

The martensite lath morphologies in the samples quenched with different media are shown in Figure 8. The laths are paralleled in quenched steel. The statistic results show that the average lath width are 359 nm, 335 nm and 302 nm for oil-quenched, water-quenched and 10% NaCl-water-quenched samples, respectively, as shown in Figure 9. The average lath width are 404 nm,

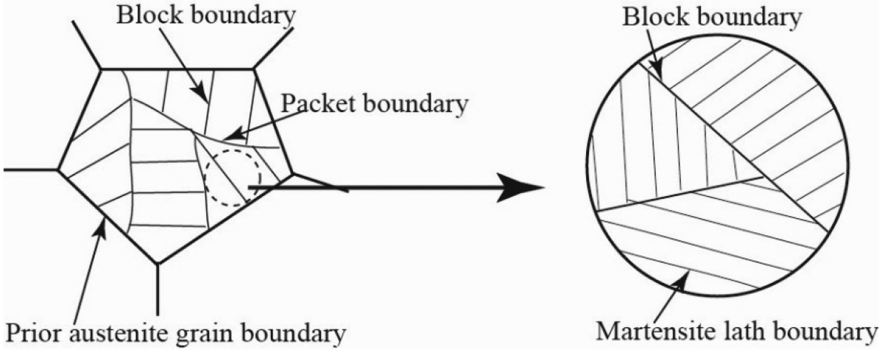

Figure 2: Schematic diagram of martensite structure [13].

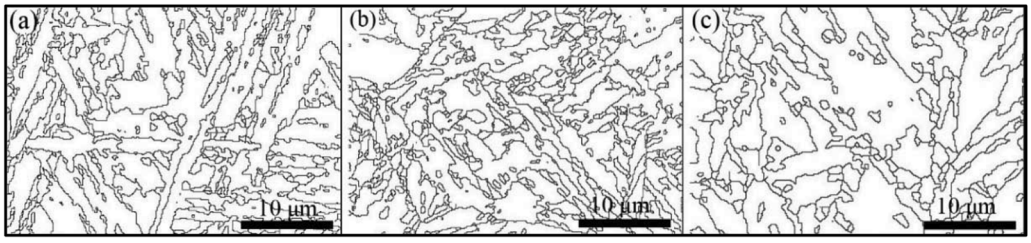

Figure 3: The martensite blocks morphology in quenched steels. (a) Oil; (b) water; (c) 10 % NaCl-water.

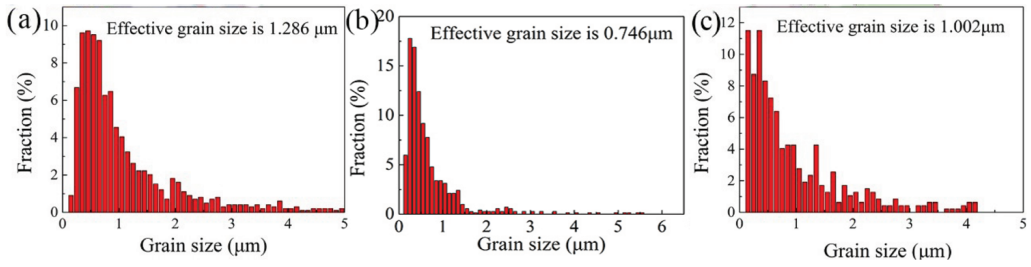

Figure 4: Grain size distribution in quenched steels. (a) Oil; (b) water; (c) 10 % NaCl-water.

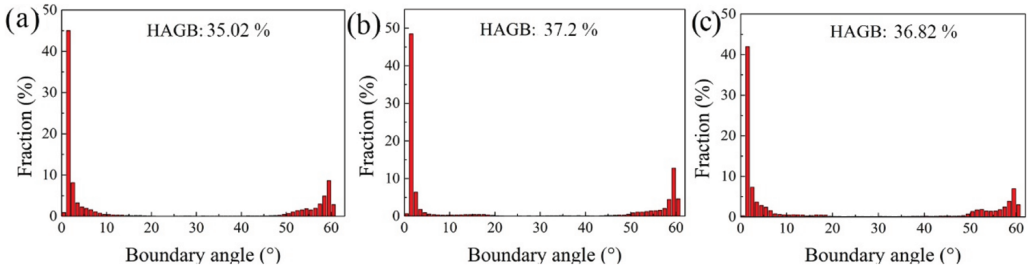

Figure 5: Grain boundary misorientation angle distribution in quenched steels. (a) Oil; (b) water; (c) 10 % NaCl-water.

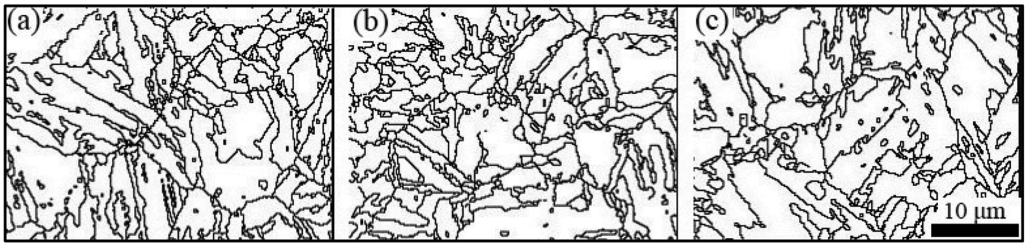

Figure 6: The martensite blocks morphology in tempered steels. (a) Oil; (b) water; (c) 10 % NaCl-water.

370 nm and 317 nm for oil-quenched, water-quenched and 10% NaCl-water-quenched and tempered samples. The lath width decreases slightly with increasing cooling rate. After tempering, the lath width increases, which is since there are laths combination due to dissolution and laths boundary movement during tempering.

The dislocation density can be determined by TEM and XRD [14–17]. TEM gives a microscopic value of dislocations, while XRD method gives a macroscopic value. The dislocations density in martensite is not uniform within a grain. Therefore, XRD method is suitable for determining dislocation density within a larger area (10 mm × 20 mm) and the result is more representative.

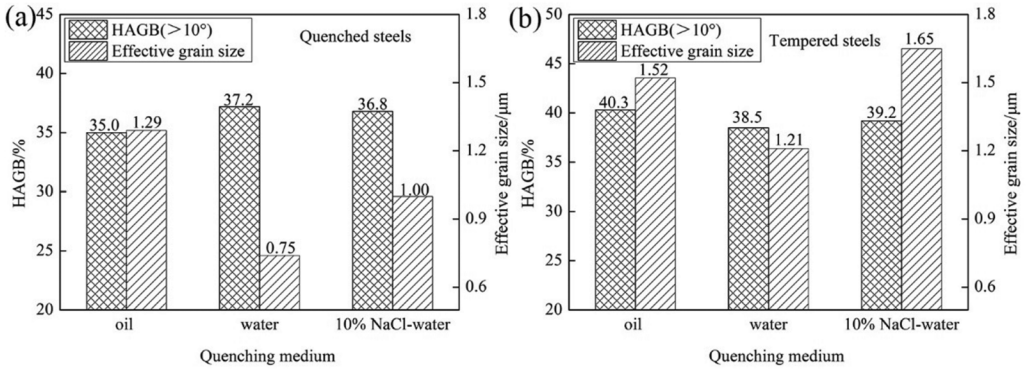

Figure 7: The influence of quenching media on effective grain size (a) quenched steels and (b) tempered steels.

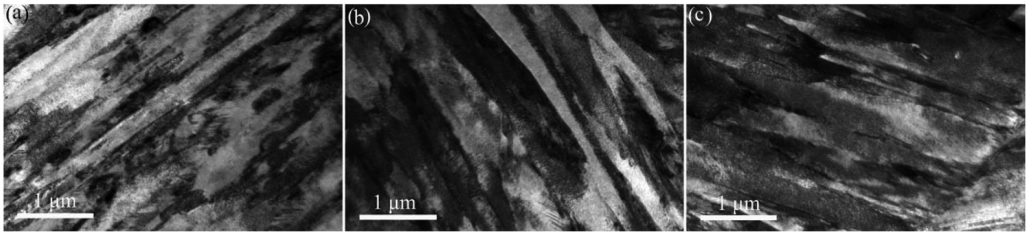

Figure 8: The martensite lath morphology in the samples quenched with different media (TEM, thin foil). (a) Oil; (b) water; (c) 10 % NaCl-water.

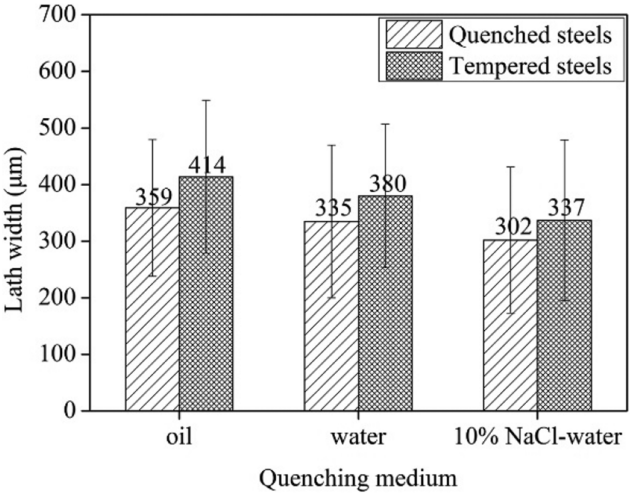

Figure 9: The influence of quenching medium on martensite lath width.

Dislocation density in the experimental steels

Dislocation density has always been characterized using the XRD peak broadening. However, strong strain anisotropy would occur in many cases and △K (XRD peak width) is not a linear function of K (diffraction vector). Therefore, the calculated results of the dislocation density through the WH method are in general slightly higher than the true values. Ungar et al. [18] took the effect of the strain anisotropy into account and put the kinematical diffraction theory of distorted crystals into use. Furthermore, they developed a modified Williamson-Hall (MWH) method. The modified Williamson-Hall (MWH) equation approximates the dislocation density from XRD peak broadening as follows [19]:

$$\Delta K \cong \frac{0.9}{D} + bM\sqrt{\frac{\pi}{2}\rho}\left(K\bar{C}^{1/2}\right) \tag{1}$$

where ΔK is XRD peak width; D is grain size; b is the Burgers vector; where M is a dimensionless constant depending on the effective cut-off radius of the dislocations; ρ is dislocation density; K is the diffraction vector; $\bar{C}$ is the dislocation constant factor for specific (hkl) diffraction, which is a function of the Miller indices through the following equations [14].

$$\bar{C} = \bar{C}_{h00}\left(1 - qH^2\right) \tag{2}$$

$$H^2 = \frac{h^2k^2 + k^2l^2 + l^2h^2}{\left(h^2 + k^2 + l^2\right)^2} \tag{3}$$

where q is a constant that depends on the type character of the dislocations and is determined experimentally. $\bar{C}_{h00}$ is the average dislocation contrast factor for the {h00} reflections determined by crystal elasticity. Here, $\bar{C}_{h00}$ is equal to 0.285 according to the literatures for pure iron materials [14]. Thus, the D value and the product $M\sqrt{\rho}$ could be got through the intercept and the slope of the MWH plot respectively, ΔK versus $K\bar{C}^{1/2}$ according to the eq. (1). The value of q can be calculated by combining eq. (1) and eq. (2) as follows [17]:

$$\frac{(\Delta K-\alpha)^2}{K^2} \cong \beta^2 \bar{C}_{h00}\left(1-qH^2\right) \tag{4}$$

Where $\alpha = 0.9/D$ and $\beta = bM\sqrt{\pi\rho/2}$. The intercept of the MWH plot, ΔK versus $K\bar{C}^{1/2}$, gives the value of α. Furthermore, the intercept of the plot, $\frac{(\Delta K-\alpha)^2}{K^2}$ versus H^2, can give the value of the dislocation density ρ by assigning a definite value to M. Generally, M is equal to 3 for iron materials.

The XRD detection results of the samples are shown in Figures 10, 11 and 12. The dislocation densities are 2.933×10^{16} cm^{-2}, 3.110×10^{16} cm^{-2} and 3.401×10^{16} cm^{-2} for oil, water and 10% NaCl-water quenched samples, respectively. The dislocation density increases with increasing cooling rate. The XRD peaks of quenched samples are obviously wider and lower than those of tempered samples, as shown in Figure 11. The dislocation density are 7.193×10^{15} cm^{-2}, 5.922×10^{15} cm^{-2} and 7.131×10^{15} cm^{-2} for oil, water and 10% NaCl-water quenched and tempered samples, respectively. The dislocation density in tempered steels is obviously less than that in quenched steel. The dislocations recovery is affected by several factors during tempering, such as pinning effect of precipitates and solution atoms segregation on dislocations. There is no obvious relationship between cooling rate and dislocation density in tempered samples. The dislocation density in water quenched and tempered sample is the lowest and it is almost the same in other two experimental steels.

Carbide precipitates in tempered steels

The quenching cooling rate not only has influence on martensite structure, but also on carbides precipitation during tempering. The carbide precipitates in tempered samples quenched with different media are shown in Figure 13. There is obvious coarsening of carbides with increasing cooling rate. The carbides area fraction and size distribution in the tempered samples are shown in Figure 14. The carbides size increases and the carbides area fraction decreases with increasing cooling rate. The carbides area fractions in Figure 14 (b) are higher than the actual volume fraction, since the samples were etched before carbon coating. Therefore, all the carbides in the volume of the etched thickness were extracted by the carbon thin film. However, the variation trend of carbides area fraction with cooling rate is still worth referencing, because the etching time is the same and the etched thickness is also almost the same for all samples.

The carbides morphologies precipitating at prior austenite grain (PAG) boundaries, lath boundaries, dislocations and matrix are shown in Figure 15. The carbides at PAG and lath boundaries are relatively large, as shown in Figures 15 (a) and (b); the carbides on dislocations are smaller than those at boundaries but larger than those in matrix, as shown in Figures 15 (c) and (d); the carbides in matrix are the smallest, as shown in Figures 15 (e) and (f).

The equilibrium precipitation in the experimental steel has been calculated by Thermo-Calc and the results are shown in Figure 16. There are $M_{23}C_6$, M_7C_3, MC, cementite, FCC-A1#1(Nb(C,N)), MnS, M_2B and BN precipitates in the steel, as shown in Figure 13 (a). $M_{23}C_6$, M_7C_3 and MC precipitate during tempering. The main elements in $M_{23}C_6$ and M_7C_3 carbides are Fe, Cr, Mo, Mn and C. MC mainly contains Mo, V and C elements. The Thermo-Calc calculation result is an equilibrium precipitation. The tempering is not an equilibrium process since the holding time is not long enough. Therefore, the calculation result may not be exactly the same with the experimental result.

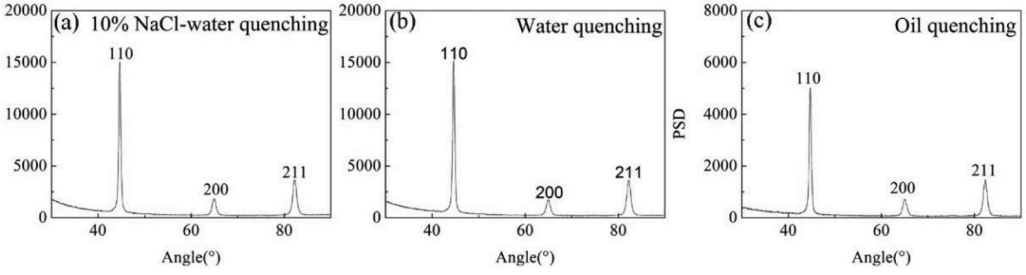

Figure 10: The XRD detection results in quenched samples. (a) 10 % NaCl-water; (b) water; (c) oil.

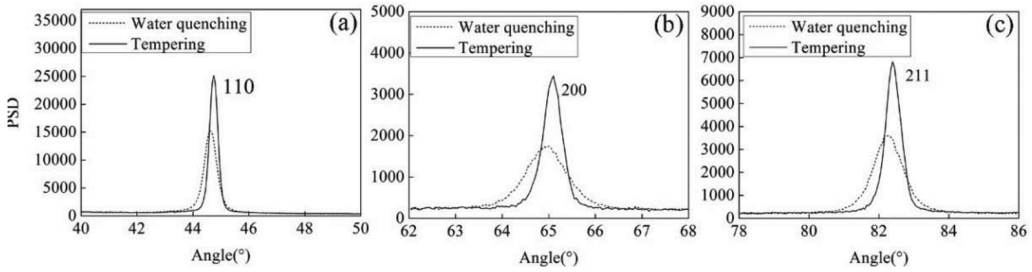

Figure 11: The comparison of peak width between water quenched sample and tempered sample. (a) 110; (b) 200; (c) 211.

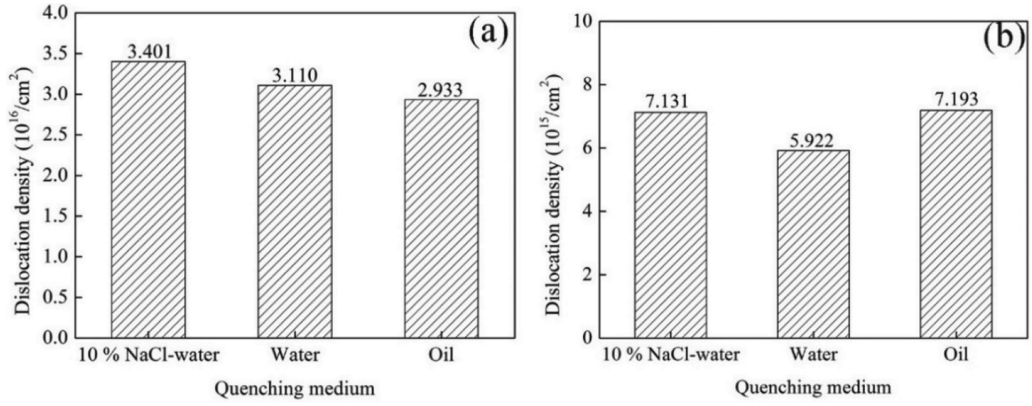

Figure 12: The dislocation density in tested steels. (a) Quenched samples; (b) tempered samples.

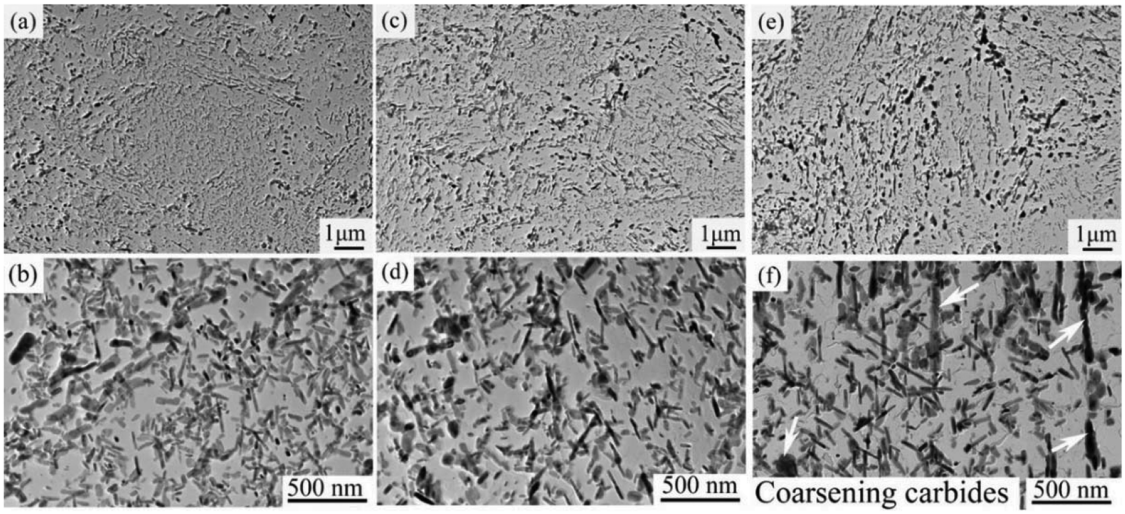

Figure 13: The carbides in tempered samples quenched with different media (TEM, carbon extraction replicas). (a) Oil; (b) water; (c) 10 % NaCl-water.

The $M_{23}C_6$ carbides in the samples form during heating and cooling process, since the heating rate and cooling rate is not fast enough to inhibit carbides precipitation.

TEM and EDS are used to analyze the carbides in the tested steels, as shown in Figure 17. Most of the carbides precipitating at boundaries of PAG and lath are $M_{23}C_6$ whose size is relatively large, as shown in Figures 17 (a) and (d). M_7C_3 carbides with a shape of round-bar are prone to precipitate in matrix, as shown in Figure 17 (g). MC carbides are also prone to precipitate in matrix and the

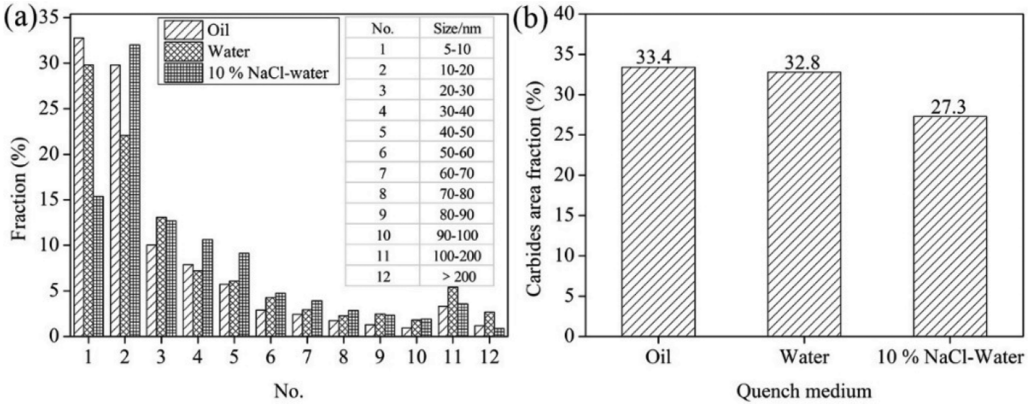

Figure 14: Carbides size distribution (a) and area fraction (b) in tempered samples with different quenching medium.

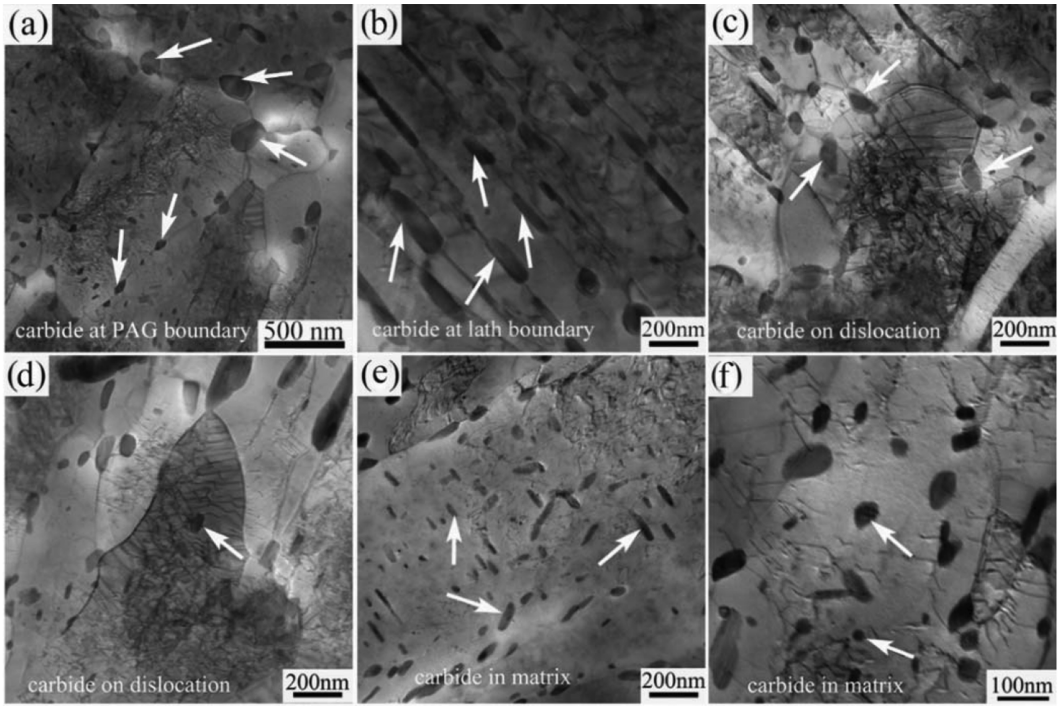

Figure 15: The precipitates morphology in water quenched and tempered sample analyzed by TEM (thin foils). (a) Carbides at PAG boundary; (b) carbides at lath boundary; (c) and (d) carbides on dislocations; (e) and (f) carbides in matrix.

size is smaller than 50 nm, as shown in Figure 17 (j). The Cu element in EDS analysis results comes from the copper net used for carbon extraction replicas preparation.

Mechanical properties of the experimental steels

The mechanical properties are shown in Table 2 and Figure 18. The tensile strength and yield strength increase slightly with increasing quenching cooling rate. The ultimate tensile strength of water quenched and tempered sample is 23 MPa higher than that of oil-quenched and tempered sample. The ultimate tensile strength of 10% NaCl-water quenched and tempered sample is only 12 MPa higher than that of water quenched and tempered sample. There is no obvious reduction of hardness and elongation. However, the impact toughness of the sample with water-quenched and tempered treatment is the best, which is 194.2 J/cm^2, and that of the sample with

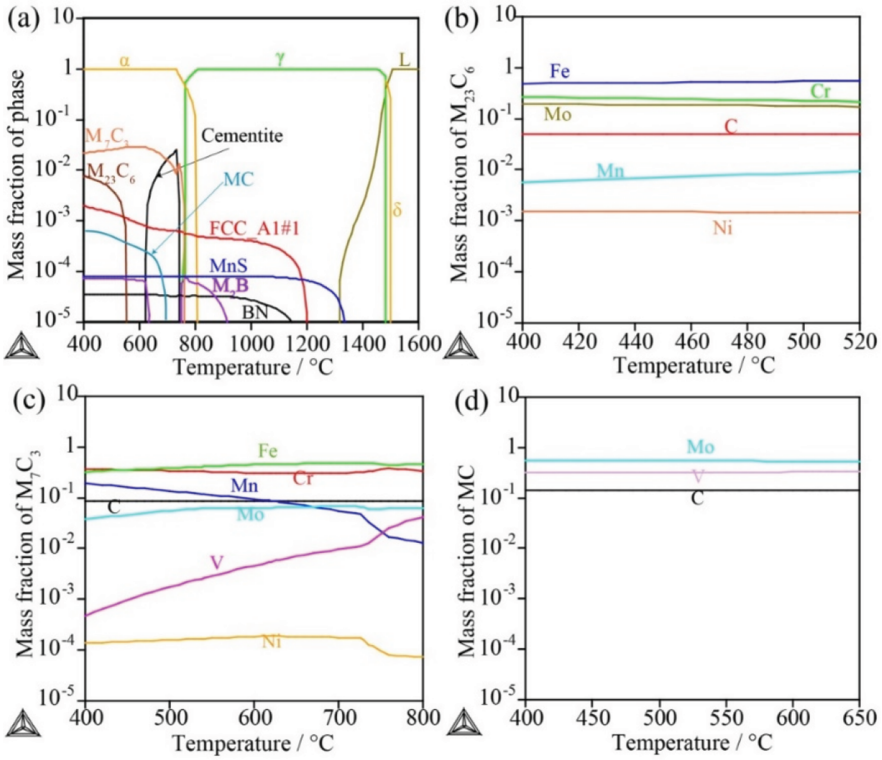

Figure 16: The results of thermodynamic calculation. (a)The equilibrium precipitation; (b), (c) and (d) the chemical compositions of $M_{23}C_6$, M_7C_3 and MC, respectively.

quenched with 10% NaCl-water and tempered treatment is the lowest, which is 172.3 J/cm^2. The comprehensive mechanical property of the water-quenched and tempered sample is the best.

Discussion

The EBSD and TEM analysis results show that the sizes of martensite structure are affected by cooling rate. The block size of the water-quenched sample is the smallest. According to solid phase transformation theory, martensite transformation is a typical representative of non-thermal activated solid phase transformation, which belongs to the first level phase transformation whose mode is nucleation and growth. The characteristic of martensite phase transformation is non-diffusion and shear transformation whose speed is very fast and controlled by nucleation. There is still dispute about martensite nucleation theory. The generally accepted view is that most of the martensite transformation is nonhomogeneous nucleation and the homogeneous nucleation only happens under special conditions [9]. According to classical nucleation theory, the nucleation ratio is illustrated as follows [9].

$$I = N_0 \omega \exp(\frac{-Q}{kT}) \exp(\frac{-\Delta G^*}{kT}) \quad (5)$$

where I is nucleation ratio; N_O is the assumed number of potential nucleus; ω is oscillation frequency of atoms which is related with surface area of nucleus; Q is the activation energy for each atom movement; $\triangle G^*$ is the activation energy for nucleation; k is Boltzmann constant; T is temperature. Although formula eq. (5) is derived from homogeneous nucleation, the form is same as nonhomogeneous nucleation. The difference is that N_O is the assumed number of potential nucleus for non-uniform nucleation and the $\triangle G^*$ is the activation energy for nonhomogeneous nucleation.

During martensitic transformation, ω and Q are considered as constant. $N_0\omega \exp(-Q/kT)$ is a parameter which decreases with increasing undercooling. The activation energy for nucleation, $\triangle G^*$, reduces exponentially with decreasing temperature. Therefore, $\exp(-\Delta G^*/kT)$ increases with decreasing temperature. The collective effect of two parameters, $N_0\omega \exp(-Q/kT)$ and$\exp(-\Delta G^*/kT)$, results in increasing of the nucleation ratio of martensite firstly and then decreaseing with increasing undercooling. The schematic diagram is shown in Figure 19. There is a

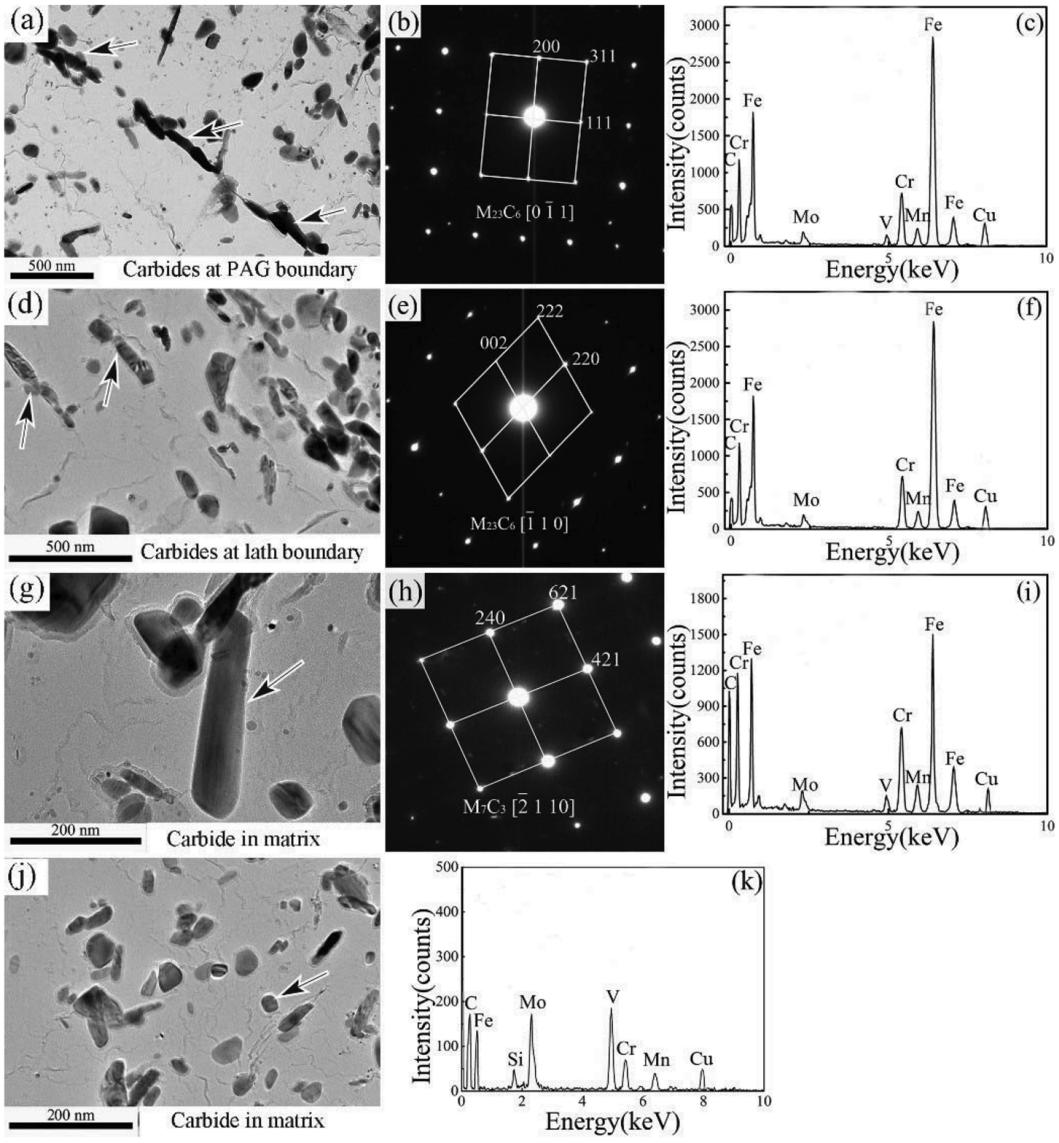

Figure 17: The morphology, SAD and EDS results of carbides. (a), (b) and (c) $M_{23}C_6$ carbides at PAG boundary; (d), (e) and (f) $M_{23}C_6$ carbides at lath boundary; (g), (h) and (i) M_7C_3 carbide in matrix; (j) and (k) MC carbide in matrix.

Table 2: The mechanical properties of the quenched and tempered samples.

Quenching media	Impact toughness J/cm^2	Ultimate tensile strength/MPa	Yield strength MPa	Hardness HRC	Elongation%
Oil	188.7 ± 8.2	957.1 ± 15.5	905.3 ± 13.1	32.6 ± 1.3	18.9 ± 0.6
Water	194.2 ± 6.9	980.3 ± 18.2	927.7 ± 14.6	33.1 ± 0.9	17.4 ± 0.5
10 % NaCl-water	172.3 ± 7.3	992.1 ± 14.9	942.6 ± 12.4	32.7 ± 1.1	17.8 ± 0.6

largest nucleation ratio with a suitable undercooling and the nucleation ratio is reduced with too small or too large undercooling. Undercooling has effect on nucleation ratio and finally influences martensitic effective grain size for nucleation controlled martensite transformation. There is a relationship between cooling rate and undercooling. The undercooling increases with increasing cooling rate due to the decreased phase transformation temperature.

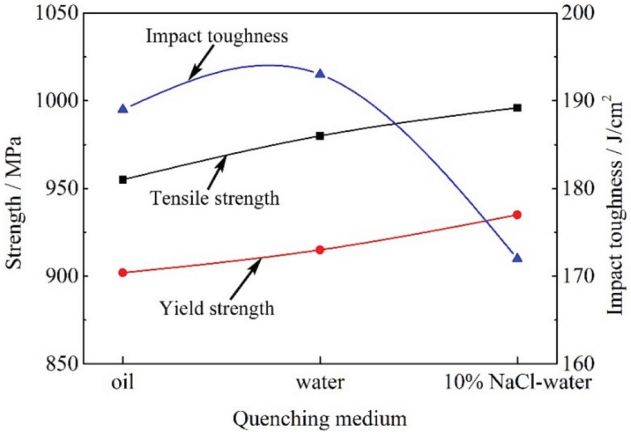

Figure 18: The mechanical properties of as quenched and tempered samples.

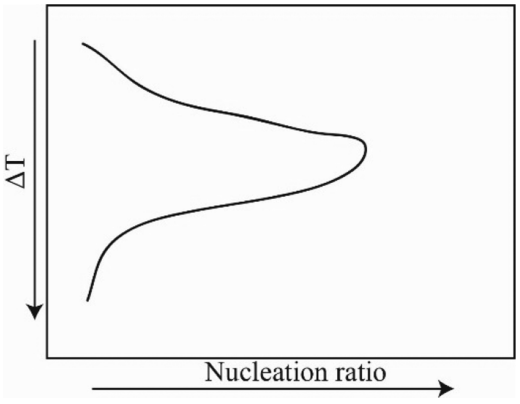

Figure 19: The schematic diagram of relationship between undercooling and nucleation ratio.

Therefore, the nucleation ratio was reduced by too slow and too fast cooling rate. From the experimental results, it is speculated that the undercooling with 10% NaCl-water quenching be over the tip of the nose in Figure 19, while with oil or water quenching below the tip of the nose.

There is an obvious coarsening of carbides in tempered samples with increasing cooling rate. Dislocations affect precipitation behavior of carbides on tempering. The alloying atoms segregate on boundaries and dislocations firstly and promote nonhomogeneous nucleation of carbides. When the cooling rate is slow, the dislocation density in the sample is relatively less. There are more lattice distortion and residual stresses in the sample with fast cooling rate. Therefore, the dislocation density is higher with fast cooling rate.

Low dislocation density reduces the amount of carbides precipitation on dislocations and promotes more carbides precipitation in matrix. However, when the cooling rate is too fast, the dislocation density in the sample increases obviously which increases the amount of carbides precipitation on dislocations. The dislocations accelerate diffusion of carbon and alloying atoms and results in coarsening of carbides. Meanwhile, the amount of small size carbides precipitation in matrix reduces.

When cooling rate is slow, the dislocations are less and the amount of large size carbides precipitated on dislocations is also less. At the same time, small carbides are homogeneously nucleated in matrix and the precipitation strengthening effect is obvious. With increasing cooling rate, the dislocation density increases, which is beneficial for improving strength, but the amount of large carbides precipitating on dislocations also increases with result of reduction of the amount of small size carbides precipitating in matrix. Therefore, the precipitation strengthening effect is reduced. In addition, the martensite structure is coarse with too fast cooling rate, which is detrimental for strength, which is the reason that the strength increment is not obvious with 10% NaCl-water quenching. The strength of water quenched and tempered sample is almost 20 MPa higher than that of oil-quench and tempered sample, because of the refined blocks and laths. The strength of 10% NaCl-water quenched and tempered sample is a little higher than that of water quenched and tempered sample, maybe because of the refined martensitic laths. The block boundary is the most effective grain boundary for strength of lath martensite, since the block boundary significantly restricts the movement of dislocations [20–23]. The martensitic lath width is also refined with increasing cooling rate. The lath boundaries can also act as barriers to dislocation movement and have a strengthening effect [23, 24].

When cooling rate is appropriate (the undercooling is near the tip of nose in Figure 19), the martensite nucleation ratio increases and get refined martensite effective grain size. The amount of high angle grain boundaries increases with martensite structure refinement which is beneficial for improving toughness. When cooling rate is too slow or too fast, the nucleation ratio is reduced which results in coarsening of effective grain size and reducing the high angle grain boundaries and deteriorates toughness.

Besides martensite structure, carbides precipitation on tempering also has effect on toughness. The carbides are coarse with fast cooling rate due to high dislocation density. During plastic deformation, there is stress concentration on large carbides which accelerates the cracks initiation. Besides, the martensite structure and the carbides are coarse with fast cooling rate. The large size carbides promote cracks initiation and coarse structure accelerates

cracks propagation. Therefore, too fast quenching cooling rate reduces impact toughness significantly.

Conclusions

The effect of cooling rate on martensite structure and carbides precipitation behavior has been investigated based on Cr-Mo alloy steel. The influence mechanism of martensite structure and carbides on mechanical properties has been analyzed. The conclusions are as follows:

(1) The martensite laths are refined and the dislocation density in quenched samples increases with increasing cooling rate. The smallest effective grain size is obtained with water cooling. The carbides are coarse in 10% NaCl-water quenched and tempered sample.

(2) The increment of strength is not significant with increasing cooling rate due to reduction of precipitation strengthening caused by carbides coarsening. 10% NaCl-water quenching deteriorates impact toughness significantly due to coarsening of martensite structure and the carbides, which is since large carbides promote cracks initiation and coarse structure accelerates cracks propagation.

Acknowledgements: The work is financial supported by National Nature Science Foundation of China under grant No.51674020 and No.51571019 and China's 13th Plan of Five-year National Key Research and Development Program under grant No. 2016YFB0300102. Dr Longfei Li has done excellent supporting work during this research.

References

[1] K.Y. Zhu, C. Oberbillig, C. Musik, D. Loison and T. Lung, Mater. Sci. Eng. A, 528 (2011) 4222–4231.
[2] H. Asahi, ISIJ Int., 42 (2002) 1150–1155.
[3] B. Hwang, D.W. Suh and S.J. Kim, Scr. Mater., 64 (2011) 1118–1120.
[4] Y.X. Zheng, F.M. Wang, C.R. Li and Y.T. He, Mater. Sci. Eng. A, 701 (2017) 45–55.
[5] D.J. Mun, E.J. Shin, Y.W. Choi, J.S. Lee and Y.M. Koo, Mater. Sci. Eng. A, 545 (2012) 214–224.
[6] M. Olasolo, P. Uranga, J.M. Rodriguez-Ibabe and B. Lopez, Mater. Sci. Eng. A, 528 (2011) 2559–2569.
[7] S. Gündüz and R.C. Cochrane, Mater. Des., 26 (2005) 486–492.
[8] S. Shanmugam, N.K. Ramisetti, R.D.K. Misra, T. Mannering, D. Panda and S. Jansto, Mater. Sci. Eng. A, 460 (2007) 335–343.
[9] X.Y. Wang, T. Pan, H. Wang, H. Su, X. Li and X. Cao, Acta. Metall. Sin, 48 (2012) 401–406.
[10] C.Y. Zhang, Q.F. Wang, J.L. Kong, G.Z. Xie, M.Z. Wang and F.C. Zhang, J. Iron Steel Res. Int., 20 (2013) 62–67.
[11] S.L. Long, Y.L. Liang, Y. Jiang, Y. Liang, M. Yang and Y.L. Yi, Mater. Sci. Eng. A, 676 (2016) 38–47.
[12] L. Cheng, Q.W. Cai, B.S. Xie, Z. Ning, X.C. Zhou and G.S. Li, Mater. Sci. Eng. A, 651 (2016) 185–191.
[13] Y.X. Zheng, F.M. Wang, C.R. Li, Y.L. Li and J. Cheng, Mater. Sci. Eng. A, 712 (2018) 453–465.
[14] S. Takebayashi, T. Kunieda, N. Yoshinaga, K. Ushioda and S. Ogata, ISIJ Int., 50 (2010) 875–882.
[15] S. Morito, J. Nishikawa and T. Maki, ISIJ Int., 43 (2003) 1475–1477.
[16] J. Pešička, R. Kužel, A. Dronhofer and G. Eggeler, Acta Mater., 51 (2003) 4847–4862.
[17] F. HajyAkbary, J. Sietsma, A.J. Böttger and M.J. Santofimia, Mater. Sci. Eng. A, 639 (2015) 208–218.
[18] T. Ungár and A. Borbély, Appl. Phys. Lett., 69 (1996) 3173–3175.
[19] Á. Révész, T. Ungár, A. Borbély and J. Lendvai, Nanostruct. Mater., 7 (1996) 779–788.
[20] S. Morito, H. Yoshida, T. Maki and X. Huang, Mater, Sci. Eng. A, 438 (2006) 237–240.
[21] A. Shibata, T. Nagoshi, M. Sone, S. Morito and Y. Higo, Mater. Sci. Eng. A, 527 (2010) 7538–7544.
[22] Y. Mine, K. Hirashita, H. Takashima, M. Matsuda and K. Takashima, Mater. Sci. Eng. A, 560 (2013) 535–544.
[23] C. Du, J. Hoefnagels, R. Vaes and M. Geers, Scripta Mater., 116 (2016) 117–121.
[24] K. Kwak, T. Mayama, Y. Mine and K. Takashima, Mater. Sci. Eng. A, 674 (2016) 104–116.